Semiconductor Physics, Quantum Electronics & Optoelectronics, 2016. V. 19, N 4. P. 352-357.
doi: https://doi.org/10.15407/spqeo19.04.352

PACS 81.05.Dz, 81.05.Rm, 81.07.St, 81.16.Be

Comparison of the synthesis routes for the ZnO/porous silica nanocomposite

G.Yu. Rudko[1], S.A. Kovalenko[1], E.G. Gule[1], V.V. Bobyk[2], V.M. Solomakha[2], A.B. Bogoslovskaya[1]
[1]*V. Lashkaryov Institute of Semiconductors Physics, NAS of Ukraine*
45, prospect Nauky, 03028 Kyiv, Ukraine; e-mail: g.yu.rudko@gmail.com
[2]*L. Pisarzhevskii Institute of Physical Chemistry, NAS of Ukraine*
31, prospect Nauky, 03028 Kyiv, Ukraine

Abstract. ZnO/porous silica nanocomposites were successfully fabricated by three different types of synthesis techniques. In all cases, the molecular sieve SBA-16 was used as a porous matrix. The *in situ* growth the nanoparticles of zinc oxide within the matrix pores was done using either gaseous or liquid precursors. The *ex-situ* method implied growing of nanoparticles in a colloidal solution with further penetration of the ripened ZnO nanoparticles into the pores of the matrix. Physico-chemical studies of the synthesized ZnO/porous silica nanocomposites showed that the introduction of zinc oxide by any of the methods did not lead to destruction of the structure of the molecular matrix SBA-16. The structure of ZnO nanoparticles, on the contrary, was strongly dependent on the growing method. The best defectless ZnO nanoparticles were obtained by *in situ* growing using gaseous precursors.

Keywords: ZnO nanoparticles, synthesis, nanoporous silica, luminescence.

Manuscript received 14.06.16; revised version received 22.08.16; accepted for publication 16.11.16; published online 05.12.16.

1. Introduction

Nanomaterials are a rapidly developing area of materials science. They are represented by one-dimensional nanowires or rods, quazi-zero-dimensional nanoparticles (NPs), which are also called quantum dots, and numerous composite materials based on the above species. Due to their small particle size and high surface-to-volume ratio NPs demonstrate various specific properties that are promising for creating new semiconductors devices. An important issue for successful applications of NPs is the stability of their characteristics. Low thermal and chemical stability can limit the practical use of NPs. One way to solve this problem is the insertion of NPs into the confining host, which would eliminate the agglomeration and prevent chemical reactions on the surface. Porous materials are an advantageous candidate for a hosting environment.

Among the porous materials, the mesoporous molecular sieves are especially attractive due to very small sizes of pores and very narrow distribution of pore sizes. Typically, the molecular sieves are synthesized from SiO_2 or Al_2O_3. The most well-known types of mesoporous silica, so to say, "classical" molecular sieves are the ones from MCM group [1, 2]. These materials are characterized by very large surface areas, ordered pore systems, and well-defined pore radius distributions. In general, any of the silica sieves has a hard framework formed by Si and O atoms that are organized into a three-dimensional network of pores and interconnecting channels with the thickness of the separating wall equal to the thickness of one SiO_2 monolayer. The shapes and size of pores and channels in different sieves vary within the range of several nanometers that makes these materials attractive as an enclosure for NPs. Recently, the SBA-type mesoporous silica attracted a great attention due to large pore sizes, thick pore walls, and better thermal and mechanical stablility than those of MCM family [3-5]. Moreover, the surfactant that is used for synthesis of these materials is

nontoxic, biodegradable, and inexpensive [6]. Among the cubic mesoporous silicas, the SBA-16 is considered to be the most attractive. SBA-16 is formed by an arrangement of spherical empty cages. Each cage is connected to eight neighbouring cages by narrow openings forming a 3D mesopores network having a body-centered cubic symmetry *Im3m*. Due to well-defined three-dimensional framework of mesopores, high specific surface area, and good thermal stability because of the thick walls inherent to SBA-16 this seave seems to be an ideal candidate for enclosing NPs.

While incorporation of NPs into molecular sieves can solve the stability and agglomeration problems, the insertion process is a challenge by itself. Various fabrication techniques to produce NPs inside the molecular sieves have been proposed, namely: wet impregnation, sol-gel method, radio-frequency sputtering, one-pot surfactant-assisted procedure, direct incorporation, grafting with organometallic compounds and others [7-15].

The variety of materials for insertion into silica-based sieves is very wide. In the present study, we focused on the semiconductor zinc oxide NPs. Nanocrystalline ZnO is one of the potential candidates for applications in optoelectronic devices [16], chemical gas sensors [17], solar cells [18], optical switches [19], as a catalyst [15], *etc.* Moreover, ZnO has been paid considerable attention as a promising electronic luminescent device material that enables producing light-emitting devices in the ultra-violet region. Thus, it is considered as a material of the next generation in LED development [20, 21].

The goal of this study is to investigate different methods of incorporation of ZnO NPs into the molecular sieve SBA-16 and to analyze the obtained ZnO/porous silica nanocomposites. The structural and luminescent properties of resulting ZnO/PS nanocomposites were studied using XRD, adsorption of *n*-hexane, and photoluminescent methods.

2. Materials and methods

2.1. Materials

For all synthesis methods the starting material for fabrication ZnO/porous silica nanocomposites was the ordered mesoporous molecular sieve SBA-16. The source materials for *in situ* growing NPs in the porous matrix were the solution of zinc nitrate $Zn(NO_3)_2$ for the wet chemical process and sublimated gaseous zinc acetylacetonate $Zn(acac)_2$ in the case of NPs growing from the gaseous phase. For the *ex-situ* method the alcoholic sol of ZnO NPs with the average size about 5.2 nm was used.

2.1.1. Synthesis of the molecular sieve SBA-16

The mesoporous silica matrix SBA-16 was synthesized using the chemical route described in [22] with application of Pluronic F127 surfactant (three-block copolymer $EO_{106}PO_{70}EO_{106}$) as a template. For the synthesis, the amount 0.57 g of Pluronic F-127 was dissolved in 26 ml of water and 4.87 g of concentrated HCl (37%). Then, 2.6 ml of TEOS were gradually added to the solution under continuous mixing. The components ratio (in moles) in the mixture of reactants was as follows: 1 TEOS:0.004 F-127:4.2 HCl:119 H_2O. This solution was permanently stirred by the magnetic mixer for 24 hours. The procedure was carried out at 60 °C. After this hydrothermal treatment, the resulting mixture was kept at 100 °C for 24 hours, and the surfactant was removed. Detemplatation was made using calcination at 550 °C in air and continued for 4-5 hours (temperature rise rate was 2 °C/min).

2.1.2. Methods of NPs synthesis within the pores of SBA-16

Introduction of zinc oxide NPs into the molecular sieve was carried out using three different methods. The main difference between synthesis methods was the route used for the ZnO NPs growth – inside or outside the molecular sieve. Correspondingly, these methods can be named *in situ* or *ex-situ* synthesis. During the *in situ* growth, the precursors are supplied into the pores either in liquid or gaseous phase, while the *ex-situ* growth implies impregnation of the sieve with ZnO NPs that have been preliminarily grown outside the matrix.

In-situ growing the NPs from gaseous precursors

The precursor of ZnO NPs for growing nanostructures from the gaseous phase is zinc acetylacetonate $Zn(acac)_2$. The physical sorption of gaseous zinc acetylacetonate in the pores of the molecular sieve is a rather slow process. Thus, one can expect formation of well-organized ensembles of ZnO NPs, provided that the pores of the sieve are well-ordered. The synthesis procedure started with calcination of molecular sieve SBA-16 in a pumped-out vessel at 350 °C for 2 hours. Afterwards, the molecular sieve in the vessel was slowly cooled down to room temperature, and the calcinated molecular sieve SBA-16 was mixed with zinc acetylacetonate (also in vacuum). Then, the temperature was increased once more up to 95 °C to achieve sublimation of zinc acetylacetonate. The gaseous zinc acetylacetonate penetrated into the pores via the diffusion process. The next step was the hydrolysis of zinc acetylacetonate inside the pores of molecular sieve to obtain ZnO. For this purpose the samples were placed into the atmosphere of water vapors and were calcinated at 550 °C for three hours.

In-situ growing the NPs from liquid precursors

Solution of zinc nitrate $Zn(NO_3)_2$ was used as a liquid precursor for impregnation of the molecular sieve by using the wet synthesis route. To make a rough estimation of the targeted content of ZnO in the molecular sieve beforehand, we started with the estimation of the moisture uptake by the matrix. The uptake was measured using the distilled water. The

corresponding value for SBA-16 is 2.5 mg. Using this value, the concentration of zinc nitrate in the solution was calculated.

The synthesis started with the dehydration of the molecular sieve SBA-16 before ZnO NPs growing. The procedure was performed at 120 °C and lasted for 2 hours. The synthesis procedure with zinc nitrate as a precursor was carried out in one step: the preliminarily dehydrated matrix was soaked in the solution of zinc nitrate for more than 2 h and then was calcinated at 550 °C for 3 h using a muffle furnace at a ramping rate of 2 °C/min.

Ex-situ method of nanocomposite synthesis by sorption of pre-grown NPs

The formation of nanocomposite started with the synthesis of NP-containing sol. The synthesis occurred in ethanol by alkali hydrolysis of the zinc acetate $Zn(CH_3COO)_2$ in the presence of NaOH. Thoroughly triturated dry $Zn(CH_3COO)_2$ and NaOH were dissolved in 45 and 5 ml of dry ethanol, correspondingly. The solutions of acetate and alkali were cooled down to 0 °C. NaOH solution was slowly drop-by-drop added to the solution of $Zn(CH_3COO)_2$ under intense mixing. The resulting product was the colorless transparent colloidal solution. The latter was kept for 2 hours at 55-60 °C for ripening. No additional stabilizers were used. The ripened ZnO colloids were stored in the darkness at 0-5 °C. The average size of ZnO NPs in the colloid was ~3.8 nm according to UV-spectroscopy data. As the size of the pores in molecular sieve SBA-16 is about 5 nm, they can accommodate the NPs of the latter size. The concentration of NPs in the as-synthesized colloid was close to $2 \cdot 10^{-2}$ mol·l^{-1}. The dehydrated molecular sieve was added to this colloidal solution and mixed during 30 minutes. The samples obtained were washed with ethanol, filtered and dried in air.

In what follows, we will label the samples in accordance with the growing method: G – for the gas phase growth, L – for the liquid phase growth, and C – for the samples obtained by introduction of NPs that were already formed in the colloidal solution into the molecular sieve.

2.2. Characterization methods

The structure and sorption properties of the obtained nanocomposites were studied using X-ray diffraction (XRD) and surface area measurements. The powder small-angle XRD patterns were recorded using the DRON-3M diffractometer equipped with the Cu Kα radiation source, λ = 1.542 Å.

The area of the inner surface in the molecular sieve was measured by hexane adsorption–desorption method using Sorptomatic 1990. The adsorption-desorption isotherms were obtained at 77 K under continuous adsorption conditions. The adsorption data were used to calculate Brunauer–Emmett–Teller (BET) specific surface area of the samples. The Barrett–Joyner–Halenda (BJH) algorithm was used to obtain the pore size distribution curves from the analysis of the adsorption branch of the isotherm.

Photoluminescence was studied at room temperature using the MDR-23 spectrometer with PMP-100 photomultiplier as a detector. The excitation sources were the N_2-laser (λ = 337 nm) and LED operating at λ = 375 nm.

3. Results and discussion

Small-angle X-ray diffraction patterns for the unloaded molecular sieve SBA-16 and ZnO-loaded nanocomposites obtained using different types of fabrication methods (curves L, G, C) are shown in Fig. 1. The pure molecular sieve SBA-16 exhibits the peak corresponding to (110) reflection 0.81° (2θ), which is typical for the cubic cage-like (*Im*3*m*) structure [23, 24].

After ZnO incorporation into molecular sieve, all the ZnO/porous silica nanocomposites exhibit very similar patterns with well-resolved diffraction peaks at 2θ about 0.80°. This is the evidence of the periodically organized mesoporous structure of the synthesized nanocomposites. The presence of the (110) reflection and insignificant change of the lattice parameter a_0 of the parent SBA-16 molecular sieve demonstrate preservation of the regular porous structure of mesoporous silica matrix. A minor variation in the position and intensity of diffraction peaks of synthesized ZnO/porous silica nanocomposites could be an indication of a violation of the regularity in the pore structure of molecular sieve. The reason for this can be somewhat uneven distribution of ZnO in the silica matrix pores as in the case of CuO inside MCM-41 [25], FeCo inside SBA-16 [7] and Pt inside SBA-15 [26].

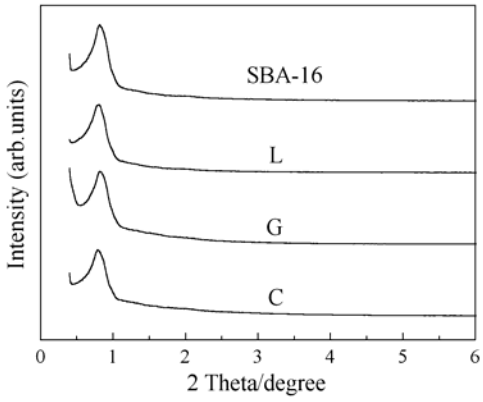

Fig. 1. The small-angle X-ray diffraction patterns for the unloaded SBA-16 (curve SBA-16) and ZnO-loaded nanocomposites obtained by growing the NPs with gaseous and liquid phase precursors (curves G and L) and by loading with NPs from the ready colloidal solution (curve C).

Semiconductor Physics, Quantum Electronics & Optoelectronics, 2016. V. 19, N 4. P. 352-357.
doi: https://doi.org/10.15407/spqeo19.04.352

Table. Textural properties of pure SBA-16 and ZnO-containing nanocomposites.

Method of ZnO loading into matrix	ZnO content, wt.%	V_{total}, cm^3/g	S_{BET}, m^2/g
Pure SBA-16	0	0.52	619
Liquid phase growth	4.95	0.30	300
Colloidal solution	2.3	0.38	328
Gas phase growth	5.3	0.33	369

Based on the analysis of small-angle X-ray diffraction pattern results, ZnO may be located in the pores of the mesoporous silica matrix or on their external surface as individual particles. The results of XRD studies of ZnO-containing nanocomposite materials within the range of angles 10…70° show the absence of the reflections related to the wurtzite ZnO structure. This fact indicates the absence of a bulk-like phase of ZnO. Thus, the size of NPs is too small for identifying them by XRD. To determine the location of the zinc oxide NPs and to compare the methods of zinc oxide introduction into silica matrix, the investigations of adsorption of *n*-hexane have been carried out for the synthesized ZnO/porous silica nanocomposites.

Fig. 2 shows the hexane absorption-desorption isotherms for the molecular sieve SBA-16 and ZnO/porous silica nanocomposites that were synthesized from the gaseous phase, liquid phase and from colloidal solution. It is seen that all isotherms demonstrate the type IV behavior, which is characteristic of adsorption by mesoporous materials [27]. The analysis of these adsorption-desorption isotherms gives us pore characteristics of pure SBA-16 and mesoporous silica nanocomposites after ZnO incorporation. The textural properties of pure SBA-16 and ZnO-containing nanocomposites calculated from experimental data are listed in Table. The calculated parameters of pure SBA-16, such as the surface area (S_{BET}) and the pore volume (V_{total}), are in good agreement with the data of [7, 28]. The decrease of pore volume with loading ZnO indicates that ZnO is indeed confined within the pores of the matrix and, thus, diminishes the free space within the pores available for hexane sorption.

Fig. 3 shows the PL spectra of ZnO/mesoporous silica nanocomposites obtained using different synthesis techniques. It should be noted that the spectrum of the ZnO/porous silica nanocomposite obtained from gaseous phase (sample G) is measured with the excitation by the 337.1 nm line of the nitrogen gas laser, while the spectra of nanocomposites obtained from liquid phase (sample L) and from colloidal solution (sample C) were measured using the 375 nm beam of the solid state laser diode. The latter spectra were also recorded under 337.1 nm excitation (not shown here), however, the signal-to-noise ratio was worse in the latter case. On the other hand, the spectrum of the sample G cannot be obtained at 375 nm excitation because the energy of quanta is not sufficient to excite PL of this sample.

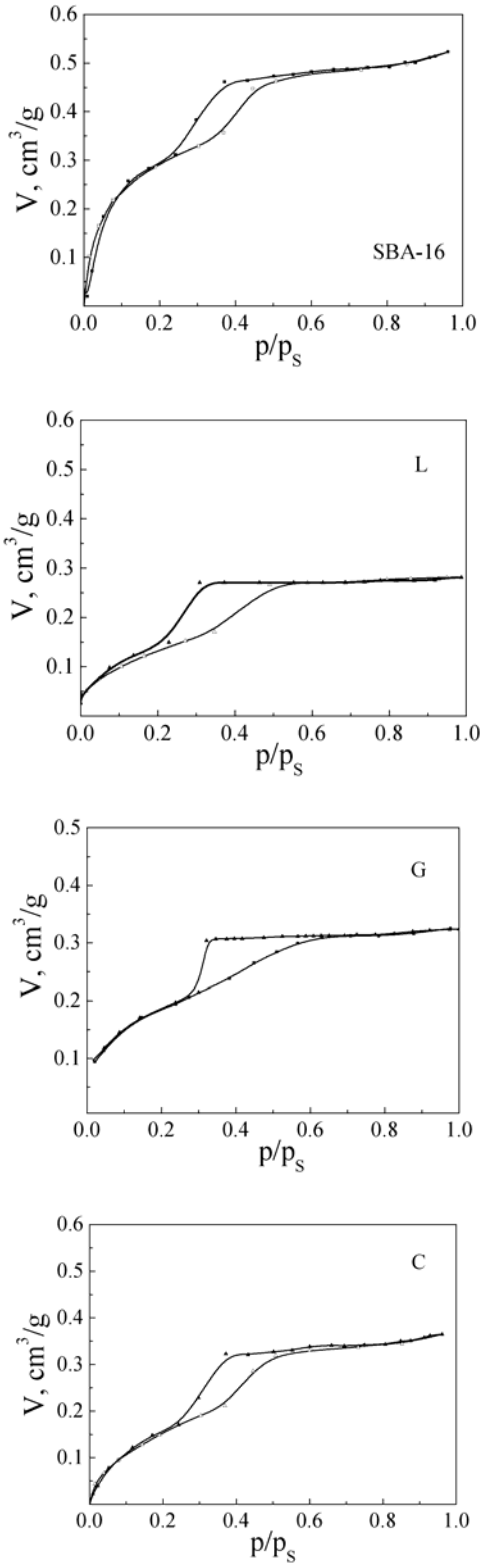

Fig. 2. Hexane adsorption–desorption isotherms for pure SBA-16 and ZnO-containing nanocomposites L, G and C.

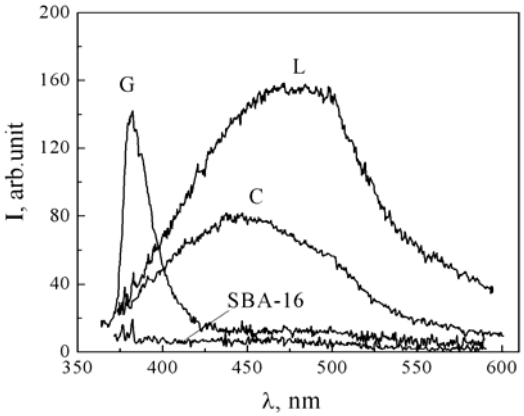

Fig. 3. Room temperature photoluminescence spectra of SBA-16 (curve SBA-16) and ZnO-containing nanocomposites G, L and C (curves G, L and C). The PL excitation source for C sample was N_2-laser ($\lambda = 337$ nm), all other samples were measured under excitation at 375 nm.

Analysis of the PL spectra (Fig. 3) shows that the pure mesoporous silica matrix SBA-16 does not emit light in the visible range, hence, the matrix does not contribute to the PL spectra of the synthesized ZnO/mesoporous silica nanocomposites. Introduction of zinc oxide into a matrix leads to a significant change of the PL spectra. Moreover, it is seen that the luminescence characteristics of nanocomposites strongly depend on the preparation method.

The nanocomposite obtained using impregnation from gaseous phase (sample G) exhibits a strong narrow luminescence line in the UV range. We attribute this luminescence line at 375 nm to the recombination of excitons in the ZnO NPs [29] that have been formed inside the pores of the silica sieve SBA-16. It should be noted that the spectrum of the sample G does not show any other features, thus, one can conclude that the quality of ZnO NPs in the nanocomposite, obtained from gaseous phase, is very high, and they do not contain any defects that may be detected using the PL technique.

PL spectra of nanocomposites, obtained from the liquid phase as well as from colloidal solution, exhibit a sufficiently broad luminescence band that is shifted to longer wavelengths. The emission maximum for the sample C is observed at 450 nm, whereas for the sample L at about 480 nm. The absence of exciton lines and the presence of very broad bands in the spectra of L and C samples indicate a worse quality of ZnO NPs. In accordance with [30, 31], we ascribe the broad PL band to the defect-related emission, the defects being presumably the vacancies of Zn.

4. Conclusions

In summary, porous silica matrix SBA-16 was successfully loaded with ZnO NPs. Three different types of synthesis techniques were used for fabrication. The *in situ* growth of NPs within the matrix pores was performed using either gaseous or liquid precursors. The *ex-situ* method implied growing the NPs in a colloidal solution with further penetration of the ripened ZnO NPs into the pores of the matrix.

The resulting nanocomposites were characterized by XRD, adsorption of *n*-hexane, and photoluminescence methods. Physico-chemical studies of the synthesized ZnO/porous silica nanocomposites showed that introduction of zinc oxide by any of the methods does not lead to destruction of the structure of the molecular matrix SBA-16 – the unit cell parameters are not changed, and no reflections related to the wurtzite ZnO structure are observed, indicating the absence of a bulk-like phase of ZnO. Adsorption methods showed the decrease of sorption volume by 30-40%. The structure of ZnO NPs, on the contrary, is strongly dependent on the growing method. The best defectless ZnO NPs were obtained using *in situ* growing with gaseous precursors; two other methods produced NPs with a lot of defects (presumably, Zn vacancies).

Acknowledgements

This work is supported by National Academy of Science of Ukraine (Project No. 6116-H).

References

1. L. Bonneviot, F. Béland, C. Danumah, Mesoporous molecular sieves, in: *Studies in Surface Science and Catalysis*, **117**, p. 614 (1998).
2. L. Huang, S. Kawi, K. Hidajat, S.C. Ng, Preparation of M41S family mesoporous silica thin films on porous oxides // *Microporous and Mesoporous Materials*, **82** (1-2), p. 87-97 (2005).
3. D. Zhao, Q. Huo, J. Feng, B.F. Chmelka, G.D. Stucky, Nonionic triblock and star diblock copolymer and oligomeric surfactant synthesis of highly ordered, hydrothermally stable, mesoporous silica structures // *J. Am. Chem. Soc.* **120**, p. 6024-6036 (1998).
4. H. Sun, Q. Tang, Y. Du, X. Liu, Y. Chen, Y. Yang, Mesostructured SBA-16 with excellent hydrothermal, thermal and mechanical stabilities: Modified synthesis and its catalytic application // *J. Colloid Interface Sci.* **333**, p. 317-323 (2009).
5. K. Cassiers, T. Linssen, M. Mathieu et al., A detailed study of thermal, hydrothermal, and mechanical stabilities of a wide range of surfactant assembled mesoporous silicas // *Chem. Mat.* **14**, p. 2317-2324 (2002).
6. H. Sun, Q. Tang, Yu Du, X. Liu, Yu. Chen, Ya. Yang, Mesostructured SBA-16 with excellent hydrothermal, thermal and mechanical stabilities: Modified synthesis and its catalytic application // *J. Colloid and Interface Sci.* **333**, p. 317-323 (2009).
7. D. Carta, M.F. Casula, S. Bullita, A. Falqui, A. Corrias, Iron–cobalt nanocrystalline alloy supported on a cubic mesostructured silica matrix: FeCo/SBA-16 porous nanocomposites // *J. Nanopart. Res.* **13**, p. 3489-3501 (2011).

8. G. Mayer, M. Fonin, U. Rudiger, R. Schneider, D. Gerthsen, N. Janben, R. Bratschitsch, The structure and optical properties of ZnO nanocrystals embedded in SiO_2 fabricated by radio-frequency sputtering // *Nanotechnology*, **20**, 075601 (2009).
9. Jamal El Haskouri, Lobna Dallali, Lorenzo Fernandez, Nuria Garro et al., ZnO nanoparticles embedded in UVM-7-like mesoporous silica materials: Synthesis and characterization // *Physica E*, **42**, p. 25-31 (2009).
10. C. Bouvy, W. Marine, B.-L. Su, ZnO/mesoporous silica nanocomposites prepared by the reverse micelle and the colloidal methods: Photo-luminescent properties and quantum size effect // *Chem. Phys.Lett*. **438**(1-3), p. 67-71 (2007).
11. P.B. Lihitkar, S. Violet, M. Shirolkar et al., Confinement of zinc oxide nanoparticles in ordered mesoporous silica MCM-41 // *Mater. Chem. and Phys.* **133**, p. 850-856 (2012).
12. K. Sowri Babu, A. Rama Chandra Reddy, Ch. Sujatha, K. Venugopal Reddy, N. Venkatathri, Structural and optical properties of ZnO nanoclusters supported on mesoporous silica // *Optoelectron. and Adv. Mater. – Rapid Communs*. **5**(9), p. 943-947 (2011).
13. Hong Cai, Honglie Shen, Linfeng Lu, Haibin Huang, Zhengxia Tang, Yugang Yin, Jiancang Shen, Properties of the ZnO/PS nanocomposites obtained by sol-gel method // *Optoelectron. and Adv. Mater. – Rapid Communs*. **4**(5), p. 650-653 (2010).
14. Vijay K. Tomer, Surender Duhan, Ashok K. Sharma, Ritu Malik, S.P. Nehrac, Sunita Devi, One pot synthesis of mesoporous ZnO – SiO_2 nanocomposite as high performance humidity sensor // *Colloids and Surfaces A: Physicochem. Eng. Aspects*, **483,** p. 121-128 (2015).
15. Supranee Lao-ubol, Rungsinee Khunlad, Siriporn Larpkiattaworn, Shih-Yuan Chen, Preparation, characterization, and catalytic performance of ZnO-SBA-15 catalysts // *Key Eng. Mater.* **690**, p. 212-217 (2016).
16. N. Izyumskaya, V. Avrutin, Ü. Özgür, Y. I. Alivov, H. Morkoc, Preparation and properties of ZnO and devices // *Phis. Status Solidi* (*b*), **244** (5), p. 1439-1450 (2007).
17. V. Aroutiounian, V. Arakelyan, V. Galstyan, K. Martirosyan, P. Soukiassian, Hydrogen sensor made of porous silicon and covered by TiO or ZnO Al thin film // *Sens J. IEEE*, **9**(1), p. 9-12 (2009).
18. Qifeng Zhang, Christopher S. Dandeneau, Xiaoyuan Zhou, Guozhong Cao, ZnO nanostructures for dye-sensitized solar cells // *Adv. Mater*. **21**, p. 4087-4108 (2009).
19. L. Martínez, O. Ocampo, Yo. Kumar, V. Agarwal, ZnO-porous silicon nanocomposite for possible memristive device fabrication // *Nanoscale Res. Lett.* **9**, p.437-443 (2014).
20. A. Kołodziejczak-Radzimska, T. Jesionowski, Zinc oxide-from synthesis to application: a review // *Materials*, **7**, p. 2833-2881 (2014).
21. A.E. Raevskaya, Ya.V. Panasiuk, O.L. Stroyuk, et al., Spectral and luminescent properties of ZnO–SiO_2 core–shell nanoparticles with size-selected ZnO cores // *RSC Adv*. **4**, p. 63393-63401 (2014).
22. F. Kleitz, D.N. Liu, G.M. Anilkumar, I.S. Park et al., Large cage face-centered-cubic Fm3m mesoporous silica: Synthesis and structure // *J. Phys. Chem. B*, **107**(51), p. 14296-14300 (2003).
23. D.Y. Zhao, Q.H. Huo, J.L. Feng, B.F. Chmelka, G.D. Stucky, Nonionic triblock and star diblock copolymer and oligomeric surfactant syntheses of highly ordered, hydrothermally stable, mesoporous silica structures // *J. Am. Chem. Soc.* **120**, p. 6024-6036 (1998).
24. W.J.J. Stevens, M. Mertens, S. Mullens et al., Formation mechanism of SBA-16 spheres and control of their dimensions // *Microporous and Mesoporous Materials*, **93**, p. 119-124 (2006).
25. X.Y. Hao, Y.Q. Zhang, J.W. Wang et al., A novel approach to prepare MCM-41 supported CuO catalyst with high metal loading and dispersion // *Microporous and Mesoporous Materials*, **88**, p. 38-47 (2006).
26. C.M. Yang, P.H. Liu, Y.F. Ho, C.Y. Chiu, K.J. Chao, Highly dispersed metal nanoparticles in functionalized SBA-15 // *Chem. Mater*. **15**(1), p. 275-280 (2003).
27. S. Brunauer, L.S. Deming, W.S. Deming, E. Teller, On a theory of the van der Waals adsorption of gases // *J. Am. Phys. Soc.* **62**, p. 1723-1732 (1940).
28. Hui Sun, Qinghu Tang, Yu Du, Xianbin Liu et al., Mesostructured SBA-16 with excellent hydrothermal, thermal and mechanical stabilities: Modified synthesis and its catalytic application // *J. Colloid and Interface Sci.* **333**, p. 317-323 (2009).
29. Qi Jiang, Zheng Ying Wu, Yi Meng Wang et al., Fabrication of photoluminescent ZnO/SBA-15 through directly dispersing zinc nitrate into the as-prepared mesoporous silica occluded with template // *J. Mater. Chem*. **16**, p. 1536-1542 (2006).
30. H.G. Chen, J.L. Shi, H.R. Chen, J.N. Yan, et al., The preparation and photoluminescence properties of ZnO-MCM-41 // *Opt. Mater*. **25**, p. 79-84 (2004).
31. Fang Na Gu, Ming Bo Yue, Zheng Ying Wu et al., Enhanced blue emission from ZnS-ZnO composites confined in SBA-15 // *J. Lumin.* **128**, p. 1148-1154 (2008).